Massachusetts Institute of Technology

Preparation of MgCo₂O₄/graphite Composites as Cathode Materials for Magnesium-ion Batteries

Siyong Gu[1], Chien-Te Hsieh[2,3]*, Mohammad Mahmudul Huq[4], Jo-Pei Hsu[2],

Yasser Ashraf Gandomi[3], Jianlin Li[5]

[1] *Fujian Provincial Key Laboratory of Functional Materials and Applications, School of Materials Science and Engineering, Xiamen University of Technology, Xiamen 361024, PR China*

[2] *Department of Chemical Engineering and Materials Science, Yuan Ze University, Taoyuan 3200, Taiwan*

[3] *Department of Mechanical, Aerospace and Biomedical Engineering, University of Tennessee, Knoxville, Tennessee 37996, USA*

[4] *Department of Chemical and Biological Engineering, University of Saskatchewan, Saskatoon, Canada*

[5] **Energy and Transportation Science Division, Oak Ridge National Laboratory, TN 37831, United States**

*   Corresponding author. Phone number: 1-865-898-0833; E-mail address: cthsieh@saturn.yzu.edu.tw (Prof. C.-T. Hsieh, Yuan Ze University) and lij4@ornl.gov (Dr. J. Li, Oak Ridge National Laboratory)

Abstract

Magnesium-ion batteries are fabricated with $MgCo_2O_4$/graphite composites as the cathode material. $MgCo_2O_4$ nanoparticles are prepared using a co-precipitation method. A three-dimensional mixing process is utilized to mechanically decorate $MgCo_2O_4$ nanoparticles on graphite particles. The $MgCo_2O_4$ spinel crystals of size ranging from 20–70 nm on micrometer sized graphite chunks are analyzed by using X-ray diffraction and scanning electron microscopy. The electrochemical properties of the as-prepared composites are well characterized by cyclic voltammetry, charge and discharge cycling, and electrochemical impedance spectroscopy (EIS). Surprisingly, the $MgCo_2O_4$/graphite composite with a relatively low proportion of $MgCo_2O_4$, compared with the other as-prepared composites, achieves the highest specific capacity of 180 mAh g^{-1} at a C rate of 0.05 C. EIS results suggest that the electrical conductivity of the composite material is an increasing function of the graphite proportion. The superior performance of the $MgCo_2O_4$/graphite composite could be ascribed to the decoration of nanosized $MgCo_2O_4$ particles as well as to the increased conductivity provided by graphite.

1. Introduction

With ever rising demand for more efficient energy storage devices, research communities worldwide are in a race to test and design batteries which can deliver higher storage in more confined space. Thus far, lithium-ion battery (LIB) has the greatest success in commercial terms, experiencing widespread application in smartphones, laptops, solar systems, electric drive vehicles etc., because of its high energy density and fast charge and discharge ability [1-3]. Yet, LIB is failing to catch up with the ever increasing energy demand of modern electronic devices [4], easily evident by the never ending rush to recharge our cell-phones or people carrying power banks (often heavier than their devices). Moreover, recent explosions of LIB devices in aircrafts and in smartphones have raised serious concerns over its future use [5, 6]. There are, however, potential alternatives to LIBs, such as non-noble polyvalent-metal (Mg, Ca, Al etc.) ion batteries, with large capacities arising from their di or tri-valence, and increased safety because of their stability in air [7-9].

Since Aurbach's seminal work in 2000, magnesium-ion battery (MIB) technology has garnered much attentions due to superior theoretical volumetric energy density of Mg^{2+} (3,832 mAh cm^{-3}) compared to that of Li^+ (2,062 mAh cm^{-3}) and low cost because of utilizing earth abundant Mg (~13.9% of earth's crust) [10-12]. Other advantages of Mg include its stability in air, and its dendrite-free deposition, preventing short circuit during fast charging, unlike Li [13]. However, one major obstacle to the development and commercialization of MIBs is the slow kinetics of Mg cations in the cathode, arising from strong polarizing nature of divalent Mg, limiting its power and energy density [14]. Moreover, only few materials allow electrochemically reversible intercalation of Mg cation, such as Chevrel phase Mo_6S_8, nano-crystalline V_2O_5 etc. [15]. Hence, currently, exploring new cathode materials for MIBs should be a priority.

MgCo$_2$O$_4$, a spinel oxide, has been demonstrated to show Mg^{2+} intercalation/de-intercalation behavior with a high open circuit voltage (OCV) [4]. The spinel oxide has been considered as electrode materials for energy storage devices such as supercapacitors using MgCo$_2$O$_4$/graphene composites [16] and LIBs using multi-shelled MgCo$_2$O$_4$ hollow microspheres [17]. As a cathode material for a MIB, with metallic Mg as an anode, MgCo$_2$O$_4$ undergoes the following reaction during charge and discharge:

Cathode: MgCo$_2$O$_4$ ↔ Mg^{2+} + Co$_2$O$_4$ + 2e$^-$ (R1)
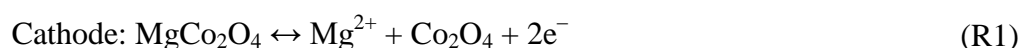
It is expected that redox reactions of Co (IV) provide high potential because of its high oxidation states. Basically, Co was chosen because it was expected to show high electrode potential because of its high oxidation state. However, the OCV rarely sustains because of the activation and concentration polarization and the internal impedance of the cell [18]. In the present work, we fabricated and studied MgCo$_2$O$_4$/graphite composites, as a cathode material for MIB for the first time. An efficient co-precipitation method is adopted to synthesize highly crystalline MgCo$_2$O$_4$ spinel nanoparticles that are homogeneously dispersed over micro-scaled graphite powders. Herein, the graphite, a highly uniform as well as a good electrically conductive material, was introduced to MgCo$_2$O$_4$-besed MIB cathode materials as an attempt to improve its performance by reducing the polarization affects and the Ohmic resistance. The novelty of the present work is to shed some lights on (i) one possibility of MgCo$_2$O$_4$ spinel crystals as cathode materials for MIBs and (ii) how weight ratio of MgCo$_2$O$_4$ to graphite affects electrochemical performance of MIBs. The unique design of MgCo$_2$O$_4$/graphite composites displays a commercial feasibility for developing high-performance MIBs.

2. Experimental

2.1 Materials

In this work, 98% pure precursors $Mg(NO_3)_2$ and $Co(NO_3)_2$ were purchased from Alfa Aesar. Graphite powders (~2 μm) were supplied by Taiwan Maxwave Co., LTD. All chemicals were used as obtained.

2.2 Materials synthesis

A co-precipitation method was adopted to synthesize $MgCo_2O_4$ nanoparticles. First, stoichiometric amount of $Mg(NO_3)_2$ and $Co(NO_3)_2$ were mixed with in 1,000 ml of de-stilled water. Afterwards, ammonia solution was added drop-wise till the pH of the solution reached a value of 9.0. Finally, H_2O_2 was introduced as a precipitating agent. After stirring for 1 h, the precipitates were removed by filtering the solution. The precipitates were then washed a few times with water to remove all the nitrates. The powders were dried in a vacuum oven overnight. In order to obtain $MgCo_2O_4$, the powders were calcined in air at 500 °C for 5 h. The $MgCo_2O_4$/graphite composites were prepared using three-dimensional mixer with zirconia ball mills. First, $MgCo_2O_4$ powders and graphite are mixed with appropriate weight ratio. The mixing process was then conducted at a high rotation speed of 4,500 rpm for 10 min, forming well-dispersed $MgCo_2O_4$ composite. Three samples with $MgCo_2O_4$ to graphite weight ratio of 7:3, 5:5 and 3:7 was prepared and designated as M7G3, M5G5 and M3G7, in order to study the effects of $MgCo_2O_4$ proportion.

2.3 Materials characterization

X-ray diffraction (XRD) spectroscope (Shimadzu labx XRD-6000) with Cu-Kα

radiation was used to study the crystalline nature of the samples. The microstructure of the sample materials was observed by using a field-emission scanning electron microscope (FE-SEM, JEOL JSM 6701F) and high resolution transmission electron microscopy (HR-TEM, FEI Talos F200s). The chemical compositions of the samples were examined using X-ray photoelectron spectroscopy (XPS). The XPS spectra were collected by Fison VG ESCA210 spectrometer and Mg-K$_\alpha$ radiation. The deconvolution of XPS spectra was conducted by a non-linear least squares fitting program with a symmetric Gaussian function.

2.4 Electrochemical characterization

Mg-ion coin cells were fabricated using the as prepared MgCo$_2$O$_4$/graphite powders as the cathode. The cathode was prepared according to the following procedure. A slurry containing active material, super P, poly-vinylidenefluoride (PVdF) with the weight ratio of 8:1:1 was prepared, using N-methyl pyrrolidinone as a solvent. In order for the slurry to be more uniform, it was blended using a three-dimensional mixer with zirconia ball mills for 3 h. Afterwards, the slurry was uniformly pasted on a stainless steel foil using a doctor blade, with the adjusted thickness of 100 μm. The weight loading for each electrode was found to be ~22 mg cm^{-2}. The electrode was then dried with a blow dryer. Coin cells were assembled using magnesium foil as the anode and porous polypropylene film as the separator. All-phenyl complex (APC) was used as the electrolyte. Cyclic voltammetry was carried out at a scan rate of 0.1 mV s^{-1} within the voltage range of 0–2.0 V. Charge and discharge measurement were performed at C rates ranging from 0.05 C to 2.0 C. After the fabrication of coin cells, the OCVs of all cells were measured first and their OCVs were approximately 1.3–1.7 V. After that, one formation process was carried

out to stabilize the coin cells by charging and discharging them at 0.02 *C* with one potential window between 0.1 and 2.0 V at ambient temperature. Electrochemical impedance spectroscopy (EIS) was conducted within the frequency range of 100 kHz to 0.01 Hz. *Z*-view software was used to simulate the equivalent circuit.

3. Results and discussion

The crystalline nature and the structural information of the as prepared MIB cathode materials were investigated by XRD spectroscopy. Figure 1 presents the XRD patterns of M3G7, M5G5 and M7G3. The characteristic graphite peak (002) appears in all samples at *2θ* angle of 26.6°, corresponding to the interlayer distance of ~0.334 nm. Conversely, the peaks corresponding to $MgCo_2O_4$ spinel structures are observed at *2θ* angles of 31.4, 36.9, 38.6, 44.8, 54.8, 59.4 and 65.4°, well indexed to (220), (311), (222), (400), (422), (511), and (440) crystal planes, respectively (JCPDS No. 02-1073). All major peaks of both graphite and $MgCo_2O_4$ are well indexed without any impurity phase appearing, and thus the formation of $MgCo_2O_4$/graphite composite is confirmed by XRD spectroscopy. The successful synthesis of $MgCo_2O_4$ can be attributed to the excellent mixing Mg-O and Co-O domains at molecular level facilitated by the co-precipitation method, which has been confirmed by pioneering study [19]. It should also be noted that, the intensity of $MgCo_2O_4$ peaks increases with the increase of $MgCo_2O_4$ proportion, as expected. The average crystallite size of $MgCo_2O_4$ nanoparticles can be estimated from XRD spectra using Debye-Scherrer equation:

$$D = k\lambda/ (\beta_{1/2} \cos \theta) \tag{1}$$

where *D* is the average crystallite size, *λ* the wavelength of the X-ray radiation

(0.15406 nm), k the Scherrer constant (0.89), and θ the Bragg angle, and $\beta_{1/2}$ the full width half maximum of the (311) diffraction peak in radians. Based on the above formula, the average crystallite sizes of M3G7, M5G5 and M7G3 samples are calculated to be 27.4, 30.5 and 32.6 nm, respectively.

FE-SEM micrographs of the as-prepared samples are presented in Figure 2(a)-2(c), presenting more magnified micrographs at different spots of the samples. As can be seen, chunk like graphite particles are in micrometer size range. As shown in HR-TEM micrographs (see Figures 2(d)-2(f)), crystalline $MgCo_2O_4$ nanoparticles with particle size ranging from 20 to 70 nm are observed in all samples. This result is in well agreement with the average crystallite size calculated by Debye-Scherrer equation. However, in some samples the $MgCo_2O_4$ particles are found to be aggregated. Overall, SEM images of the as-prepared samples confirm the excellent efficiency of the three-dimensional mixing method in decorating nanoparticles on graphite. As shown in Figure 3, the elemental mappings obtained from the SEM images show the uniform distribution of Co, Mg and O on graphite, implying the formation of pure $MgCo_2O_4$ without any impurities. Moreover, C element is also homogenously distributed, further demonstrating that graphene thin film was well retained.

Besides XRD, high-resolution XPS scan on Co 2p of the $MgCo_2O_4$/graphite samples has been presented in Figures 4 (a)-4(c), signifying formation of $MgCo_2O_4$. The XPS spectra of Co 2p peaks show several symmetric peaks, which consist of overlapping features originating from the $2p_{3/2}$ and $2p_{1/2}$ peaks due to Co^{2+} and Co^{3+} together with the associated satellite structure. The peaks at 782.1 and 796.9 eV are related with Co^{3+} component and the peaks located at 780.2 and 795.5 eV are related with Co^{2+} component in $MgCo_2O_4$ crystals [16]. The satellite peak located at

786.3–789.5 eV is associated with Co^{2+} species and Co^{3+} component, whereas the satellite peak located at 803.1 eV is associated with Co^{2+}/Co^{3+} [20,21]. Therefore, both Co^{2+} and Co^{3+} exist in as-prepared $MgCo_2O_4$/graphite composites. The O 1s spectra (see Figures 4(d)-4(f)) can be deconvoluted into three peaks at 529.8 and 531.6 eV [22]. From a semi-quantitative point of view, the peaks, occurred at 529.7 and 531.6 eV, are main contributors to O 1s spectra. The peak with lower binding energy (529.7 eV) was generally assigned to a normal O 1s (O^{2-}) signal, which corresponds to the lattice oxygen type. The peak with higher binding energy (531.8 eV) mainly originates from adsorbed oxygen, in the form of O^-, which is weakly bound to the spinel surface. It can easily be noticed that all spinel crystals prepared by the co-precipitation method are able to provide a number of O^- species on the surface. The above results indicate that the as-prepared $MgCo_2O_4$ spinel crystals are pure phase and the graphene is well retained, supporting the results of XRD, SEM mapping, HR-TEM, and XPS analyses.

The cyclic voltammogram (CV) of M3G7, M5G5 and M7G3 electrodes are presented in Figures 5(a), 5(b) and 5(c), respectively. The presented CV curves were taken after one charge and discharge sweep. The voltage sweep was done at a rate of 0.1 mV s^{-1} within the voltage range of 0–2.0 V vs. Mg/Mg$^+$. All three samples show anodic and cathodic peaks at 1.29 and 0.25 V vs. Mg/Mg$^+$, respectively. The corresponding Mg^{2+} de-intercalation/intercalation reactions during charge and discharge could be expressed as follows

$$MgCo_2O_4 \leftrightarrow Mg_{1-x}Co_2O_4 + x(Mg^{2+} + 2e^-) \qquad\qquad (R2)$$
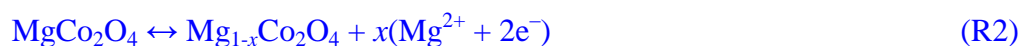
The intensities of the CV peaks are found to be an increasing function of the graphite proportion.

Figure 6(a), 6(b), 6(c) and 6(d) present the charge and discharge curves of

M3G7, M5G5, M7G3, and pristine graphite cathode, respectively, at C rates ranging from 0.05 C to 2.0 C within a potential range of 0–2.0 V. Among the electrodes, sample M3G7 shows the highest specific capacity of 180 mAh g^{-1} at 0.05 C. Surprisingly, the specific capacity falls as the proportion of $MgCo_2O_4$ increases, with M7G3 showing a capacity value of 78 mAh g^{-1} at 0.05 C. This result can be attributed to the aggregation of nanoparticles at increased $MgCo_2O_4$ content. Interestingly, graphite, a seemingly inactive cathode material, shows a specific capacity of 29 mAh g^{-1}. This capacity probably originates from the formation of electric double-layers on graphite surface. The capacity of each sample is found to be a decreasing function of the C rate, confirming the presence of ionic diffusion resistance during the Mg-insertion/extraction process.

The theoretical capacity of spinel $MgCo_2O_4$ can attain as high as 260 mAh g^{-1} when Mg ions are totally inserted into and extracted from the $MgCo_2O_4$ crystal, i.e., the redox reaction of R1: $MgCo_2O_4 \leftrightarrow Mg^{2+} + Co_2O_4 + 2e^-$. This is an ideal condition to reach high energy density of $MgCo_2O_4$-besed MIB. However, the M3G7 electrode achieves the highest specific capacity of 180 mAh g^{-1} at 0.05 C, which is lower than the theoretical capacity (260 mAh g^{-1}). However, the specific capacity is superior to that of $MgMn_2O_4$-based electrode, i.e., 169 mA h g^{-1} at 0.0139 C [23]. This reveals that Mg ions are partially inserted into and extracted from the spinel crystal, referring to R2: $MgCo_2O_4 \leftrightarrow Mg_{1-x}Co_2O_4 + x(Mg^{2+} + 2e^-)$, where x value is approximately 69.2%. Accordingly, R2 provides a better description to the redox reaction in $MgCo_2O_4$-besed MIB. This disappearance in the maximal capacity can be attributed to poor electrical conductivity of $MgCo_2O_4$ and difficult extraction of Mg ions in the $MgCo_2O_4$ crystals due to strong bonding in the spinel oxides.

Figure 7(a) illustrates the rate capability of the as-prepared cathode materials at

different C rates ranging from 0.05 to 1.0 *C*. As the *C* rate is increased, the specific capacity of all samples starts dropping gradually, i.e., M3G7 experiences a drop from 180 to 34 mAh g^{-1}, M5G5 from 175 to 15 mAh g^{-1} and M7G3 from 78 to 5 mAh g^{-1}, once the *C* rate is increased from 0.05 to 1.0 *C*. However, all three samples recovered nearly 95% of their initial specific capacities when the *C* rate is reduced back to 0.05 *C* on the 15th cycle, clearly indicating that the composite structures stayed stable during repetitive charge and discharge cycles. This is also confirmed by the cyclic performance test in which M3G7 retained nearly 90 % of its initial capacitance when charged and discharged for 30 cycles at 0.05 *C*, as depicted in Figure 7(b). The excellent cyclic performance of M3G7 can be attributed to its distinct structure, nano-sized particles, and improved electrical conductivity; relieving the stress arising from volume changes of the nanoparticles during repetitive charge and discharge.

Since MgCo$_2$O$_4$ crystals were coated over graphite, the ionic diffusion resistance is thus, strongly dependent to the surface loading of MgCo$_2$O$_4$ crystals. At low loading of MgCo$_2$O$_4$ crystals, surface coverage of MgCo$_2$O$_4$ crystals can be highly utilized due to small diffusion resistance and well contact to conductive graphite powders. It can be observed from Figure 2 that there are serious aggregations onto graphite surface at high surface loading. As to high loading, when the *C* rate is low, agglomerated MgCo$_2$O$_4$ particles, although not in contact with graphite directly, can participate in the electrochemical reactions because both ionic transport electron transport can take place through the agglomerated spinel crystals themselves and then to the MgCo$_2$O$_4$ particles in contact with graphite. However, this phenomenon cannot stand, when the *C* rate is relatively high, because of low electronic conductivity of MgCo$_2$O$_4$ particles. This finding is also observed on Na$_3$MnCO$_3$PO$_4$-based electrodes in sodium ion batteries [24].

Figure 8(a) presents the Nyquist plots for the as-prepared cathode materials, obtained from EIS measurements within the frequency range from 0.01 to 100 kHz in order for making a comparison of their electrical conductivities. Each Nyquist plot can be divided into three sections: (i) an intersection in the real axis in high frequency region, indicating the bulk solution resistance of the system, (ii) a semicircle, whose diameter represents the charge transfer resistance and (iii) a slant line in the low frequency region, whose slope is the representative of the diffusion coefficient of the ions inside the electrode structure [25,26]. Figure 8(b) illustrates a proposed equivalent circuit for the as-prepared MIB system, where R_S represents the resistance imposed by the electrolyte, R_{SEI} the resistance of the solid electrolyte interface (SEI) film adjacent to the electrode, formed by the oxidation and reduction products of the electrolyte, R_I the interfacial resistance, R_{CT} the charge transfer (CT) resistance, encapsulating activation polarization, and W the Warburg impedance, representing the resistance to ionic diffusion. C_{SEI}, C_I and C_{CT} represent the constant phase elements of the capacitance arising from SEI film, double layer at the interface and CT, respectively. The resistance values obtained by simulating the equivalent circuit with Z-view software are presented in Table 1. The equivalent series resistance ($R_{ES}= R_S + R_{SEI} + R_I + R_{CT}$) of the as-prepared cathode materials follows an order of M3G7 (82.3 Ω) < M5G5 (158.2 Ω) < M7G3 (250.1 Ω). As can be seen, the R_{ES} values of the materials are primarily dominated by R_{SEI} and R_{CT} values, i.e., 72 to 91% of the R_{ES} values. On the other hand, R_S understandably remains fairly constant for all cathode materials and R_I is insignificant in comparison with other resistances. R_{CT} value is found to be a decreasing function of the proportion of graphite, implying that the presence of graphite, an excellent electrical conductor, increases the possibility of electron injection and extraction from $MgCo_2O_4$/graphite composite. This increased

conductivity can also be explained by the percolation theory. According to this theory, a composite material consisting of equally sized insulating and conducting particles obtained a conductive network when conducting material volume proportion is above 28.6% [27]. This threshold increases when the insulating particle size is smaller than that of conducting particles. In other words, less volume proportion of insulating material leads to more developed conductive networks, which could explain why M3G7 shows significantly better conductivity thus higher specific capacity than the other samples that have lesser proportion of conducting material. Similarly, R_{SEI}, also decreases as graphite proportion increases. Although, the chemistry of the formation SEI film on the cathode is poorly understood thus far, as compared to that of SEI film on the anode. It is generally accepted that the film is formed by the oxidation products of the electrolyte, leading to formation of resistive electrical paths and pore plugs in the cathode structure [24,28]. The simulation results indicate that the SEI film on the cathode is suppressed as the proportion of graphite increases. The Randles plots for the electrodes are shown in Figure 9, relating angular frequency ($\omega^{-1/2}$) to real impedance (Re Z'). The diffusion coefficient of the electrolyte ions can be calculated using the following equation [30].

$$D = \left(\frac{RT}{\sqrt{2}F^2 \sigma C} \right)^2 \qquad (2)$$

where D is the diffusion coefficient, R the gas constant, T the absolute temperature, A the electrode area, F the Faraday's constant, C_A the electrolyte concentration, and σ the coefficient of Warburg impedance, represented by the slope of the Randles plot. Herein, fourteen final points at the low frequency region of the Randles plot are considered in the calculation. The as calculated diffusion co-efficient for the as prepared electrodes are of order: M3G7 (1.93×10^{-12} cm^2 s^{-1}) > M5G5 (1.43×10^{-12} cm^2

s^{-1}) > M7G3 (1.08$\times$10^{-12} cm^2 s^{-1}), which is in agreement with the order of average crystallite size of the samples, calculated from Debye-Scherrer formula. Basically, reduced crystallite size of MgC$_2$O$_4$ provides more porosity, leading to better diffusion; in addition to offering more active surface area to the electrolytes. Overall, the above experiments suggest that, as a cathode material for MIBs, MgCo$_2$O$_4$/graphite composites offer a superior capacity as well as excellent charge and discharge performance, arising from its distinct structure, nano-sized particles, and improved electrical conductivity.

4. Conclusions

MgCo$_2$O$_4$/graphite composite cathodes were prepared for MIB application. Electrochemical studies revealed that, the decoration of MgCo$_2$O$_4$ nanoparticles on micrometer sized graphite particles gives rise to excellent capacity performance. Interestingly, M3G7 showed the highest specific capacity, despite having the lowest proportion of MgCo$_2$O$_4$. The rate capability study of the cathode materials showed an excellent capacity recovery of around 95%. EIS analysis suggested that the introduction of graphite significantly enhance the electrical conductivity of the cathode material, increasing the possibility of electron injection and extraction from the electrode material, suppressing the SEI film formed on the cathode, and enabling faster diffusion of electrolytes. In summary, MgCo$_2$O$_4$/graphite composite is a potential candidate as a cathode material for MIBs, because of its superior specific capacity and excellent rate capability, arising from its distinct structure, nano-sized particles, and improved electrical conductivity. To speed up commercial feasibility, future work regarding high rate capability, appropriate electrolyte, and pilot-scale

synthesis method still requires an in-depth investigation in the near future.

References

[1]   Bucur CB, Gregory T, Oliver AG, Muldoon J (2015) Confession of a magnesium battery, J. Phys. Chem. Lett. 6: 3578-3591.

[2]   Saha P, Jampani PH, Datta MK, Okoli CU, Manivannan A, Kumta PN (2014) A convenient approach to Mo_6S_8 Chevrel phase cathode for rechargeable magnesium battery, J Electrochem Soc 161: A593-8.

[3]   Liu B, Luo T, Mu G, Wang X, Chen D, Shen G (2013) Rechargeable Mg-ion batteries based on WSe_2 nanowire cathodes, ACS Nano 7: 8051-8058.

[4]   Okamoto S, Ichitsubo T, Kawaguchi T, Kumagai Y, Oba F, Yagi S, Shimokawa K, Goto N, Doi T, Matsubara E (2015) Intercalation and push-out process with spinel-to-rocksalt transition on Mg insertion into spinel oxides in magnesium batteries, Adv. Sci. 2: 1500072.

[5]   www.samsung.com
        http://www.samsung.com/us/note7recall/. (Accessed 10 June, 2017).

[6]   Scientific American
        https://www.scientificamerican.com/article/how-lithium-ion-batteries-grounded-the-dreamliner/. (Accessed 10 June, 2017).

[7]   Besenhard JO, Winter M (2002) Advances in battery technology: rechargeable magnesium batteries and novel negative-electrode materials for lithium ion batteries, ChemPhysChem 3: 155-159.

[8]   Padigi P, Goncher G, Evans D, Solanki R (2015) Potassium barium hexacyanoferrate-a potential cathode material for rechargeable calcium ion batteries, J. Power Sources 273: 460-464.

[9]   Jayaprakash N, Das SK, Archer LA (2011) The rechargeable aluminum-ion battery, Chem. Commun. 47: 12610-12612.

[10]   Aurbach D, Lu Z, Schechter A, Gofer Y, Gizbar H (2000) Prototype systems for rechargeable magnesium batteries, Nature 407: 724.

[11]   Matsui M (2011) Study on electrochemically deposited Mg metal, J. Power Sources 196: 7048-7055.

[12]   Kim HS, Arthur TS, Allred GD, Zajicek J, Newman JG, Rodnyansky AE, Oliver AG, Boggess WC, Muldoon J (2011) Structure and compatibility of a magnesium electrolyte with a sulphur cathode, Nat. Commun. 2: 427.

[13]   Z. Chang, Y. Yang, X. Wang, M. Li, Z. Fu, Y. Wu, R. Holze, Hybrid system for rechargeable magnesium battery with high energy density, Sci. Rep. 5 (2015) 11931.

[14]   Cheng Y, Shao Y, Zhang JG, Sprenkle VL, Liu J, Li G (2014) High performance batteries based on hybrid magnesium and lithium chemistry, Chem. Commun. 50: 9644-9646.

[15]   Ichitsubo T, Adachi T, Yagi S, Doi T (2011) Potential positive electrodes for high-voltage magnesium-ion batteries, J. Mater. Chem. 21: 11764-11772.

[16]   Guan X, Wang Q, Luo P, Yu Y, Li X, Zhang Y, Chen D (2018) Morphology-tuned synthesis of $MgCo_2O_4$ arrays on graphene coated nickel foam for high-rate supercapacitor electrode. Int. J. Electrochem. Sci. 13: 2272-2285.

[17]   Shin H, Lee WJ (2016) Multi-shelled $MgCo_2O_4$ hollow microspheres as anodes for lithium ion batteries. J. Mater. Chem. A 4: 12263-12272.

[18]   Liu C, Neale ZG, Cao G (2016) Understanding electrochemical potentials of cathode materials in rechargeable batteries, Mater. Today 19: 109-123.

[19]   Wang C, Shaw LL (2014). On synthesis of Fe_2SiO_4/SiO_2 and Fe_2O_3/SiO_2 composites through sol-gel and solid-state reactions, J. Sol-Gel Sci. Technol. 72, 602-614.

[20] Stelmachowski P, Maniak G, Kaczmarczyk J, Zasada F, Piskorz W, Kotarba A, Sojka Z (2014) Mg and Al substituted cobalt spinels as catalysts for low temperature deN$_2$O-evidence for octahedral cobalt active sites. Appl. Catal. B: Environ. 146: 105.

[21] Pu ZY, Zhou H, Zheng YF, Huang WZ, Li XN (2017) Enhanced methane combustion over Co$_3$O$_4$ catalysts prepared by a facile precipitation method: effect of aging time. Appl. Surf. Sci. 410: 14.

[22] Zamudio MA, Bensaid S, Fino D, Russo N (2011) Influence of the MgCo$_2$O$_4$ preparation method on N$_2$O catalytic decomposition, Ind. Eng. Chem. Res. 50: 2622-2627.

[23] Truong QD, Devaraju MK, Tran PD, Gambe Y, Nayuki K, Sasaki Y, Honma I (2017) Unravelling the surface structure of MgMn$_2$O$_4$ cathode materials for rechargeable magnesium-ion battery. Chem. Mater. 29: 6245-6251.

[24] Wang C, Sawicki M, Emani S, Liu C, Shaw LL (2015). Na$_3$MnCO$_3$PO$_4$-a high capacity, multi-electron transfer redox cathode material for sodium ion batteries. Electrochimica Acta, 161: 322-328.

[25] Huq MM, Hsieh CT, Lin ZW, Yuan CY (2016) One-step electrophoretic fabrication of a graphene and carbon nanotube-based scaffold for manganese-based pseudocapacitors, RSC Adv. 6: 87961-87968.

[26] Huq MM, Hsieh CT, Ho CY (2016) Preparation of carbon nanotube-activated carbon hybrid electrodes by electrophoretic deposition for supercapacitor applications, Diamond Relat. Mater. 62: 58-64.

[27] Wang Y, Guo X, Greenbaum S, Liu J (2001) Solid electrolyte interphase formation on lithium-ion electrodes: a 7Li nuclear magnetic resonance study, Electrochem. Solid-State Lett. 4: A68-A70.

[28] Lei J, Li L, Kostecki R, Muller R, McLarnon F (2005) Characterization of SEI layers on LiMn$_2$O$_4$ cathodes with in situ spectroscopic ellipsometry, J. Electrochem Soc 152: A774-A777.

[29] Wang C, Sawicki M, Kaduk JA, Liu C, Shaw LL (2015). Roles of processing, structural defects and ionic conductivity in the electrochemical performance of Na$_3$MnCO$_3$PO$_4$ cathode materials. J. Electrochem. Soc., 162: A1601-A1609.

[30] Shi M, Chen Z, Sun J (1999) Determination of chloride diffusivity in concrete by AC impedance spectroscopy, Cem. Concr. Res. 29: 1111-1115.

Table 1. EIS simulation parameters of different composite anodes

Electrode	$R_S\ (\Omega)$	$R_{SEI}\ (\Omega)$	$R_I\ (\Omega)$	$R_{CT}\ (\Omega)$
M3G7	18.3 (22%)	25.6 (31%)	4.9 (6%)	33.5 (41%)
M5G5	23.0 (15%)	52.2 (33%)	13.8 (8%)	69.2 (44%)
M7G3	20.1 (8%)	100.2 (40%)	3.4 (1%)	126.4 (51%)

Figures Caption
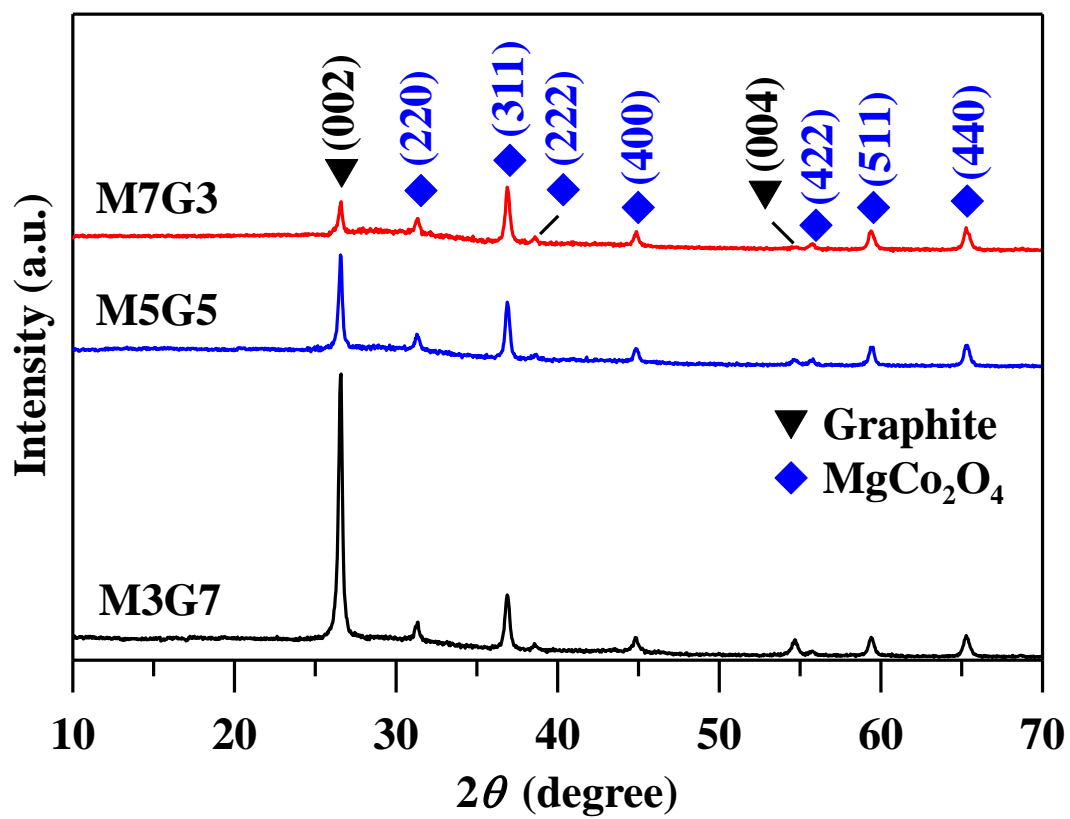
Fig. 1.   Typical XRD patterns of different composite cathodes

Fig. 2.   FE-SEM micrographs of $MgCo_2O_4$/graphite composites with low and high magnifications: (a,d) M3G7, (b,e) M5G5 and (c,f) M7G3 samples.

Fig. 3.   TEM images and elemental mapping pictures of (a) M3G7 (b) M5G5 and (c) M7G3 samples, showing the presence and the distribution of C, Co, Mg, and O elements on $MgCo_2O_4$/graphite composites.

Fig. 4.   XPS scan on Co 2p of $MgCo_2O_4$/graphite composites: (a) M3G7, (b) M5G5, and (c) M7G3. XPS scan on O 1s of $MgCo_2O_4$/graphite composites: (d) M3G7, (e) M5G5, and (f) M7G3.

Fig. 5.   Typical CV curves of (a) M3G7, (b) M5G5 and (c) M7G3 electrodes

Fig. 6.   Typical charge-discharge cycling curves of (a) M3G7, (b) M5G5, (c) M7G3 and (d) graphite electrodes at different C rates

Fig. 7.   (a) The discharge capacity of $MgCo_2O_4$/graphite electrodes as a function of cycle number at different C rates. (b) Cyclic stability of $MgCo_2O_4$/graphite electrodes charged and discharged at 0.05 C.

Fig. 8.   Electrochemical impedance spectroscopy of composite cathodes: (a) Nyquist plots and (b) equivalent circuit

Fig. 9.   Randles plot of M3G7, M5G5 and M7G3 electrodes

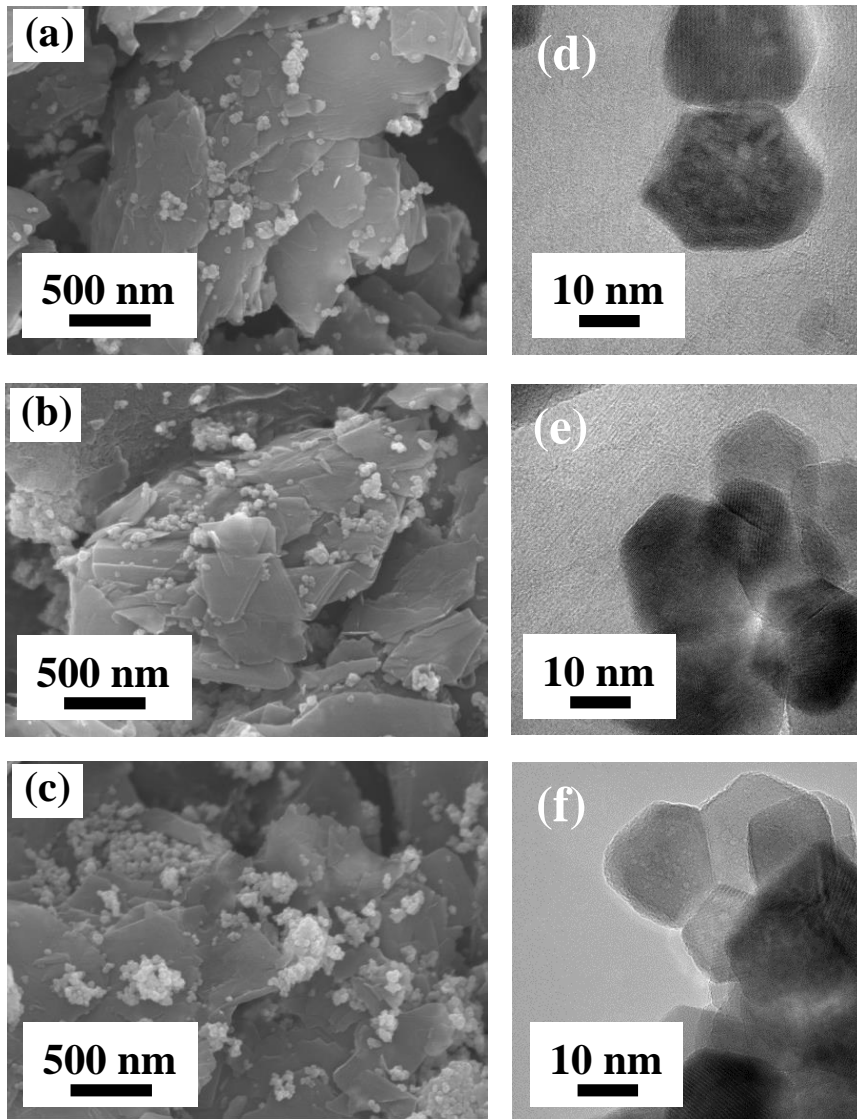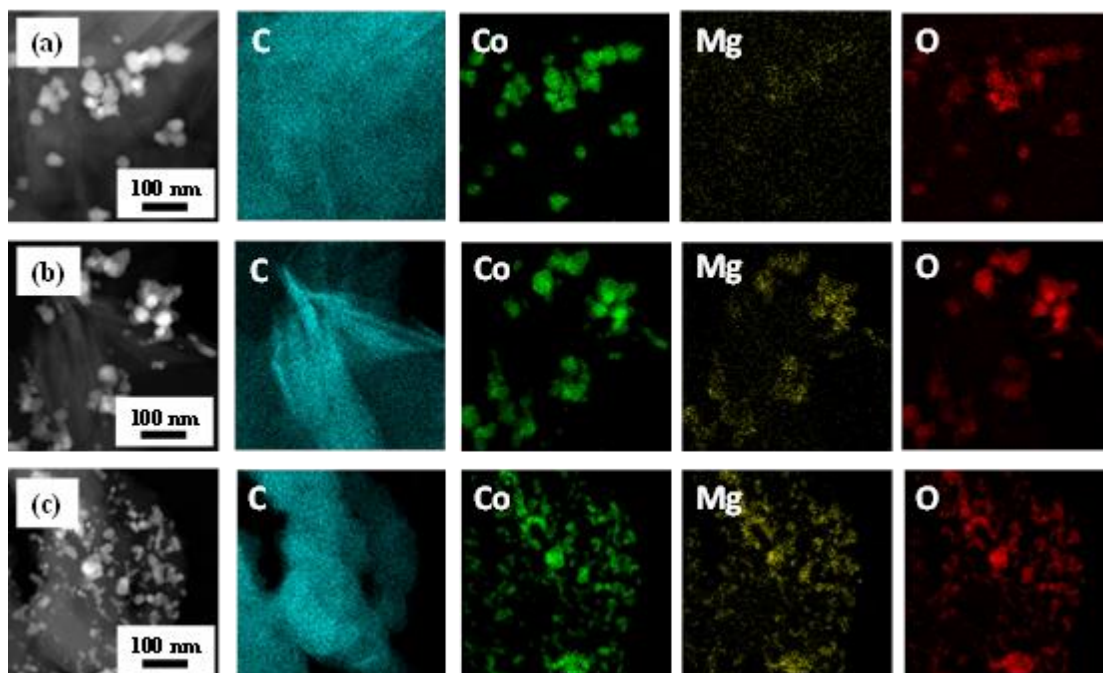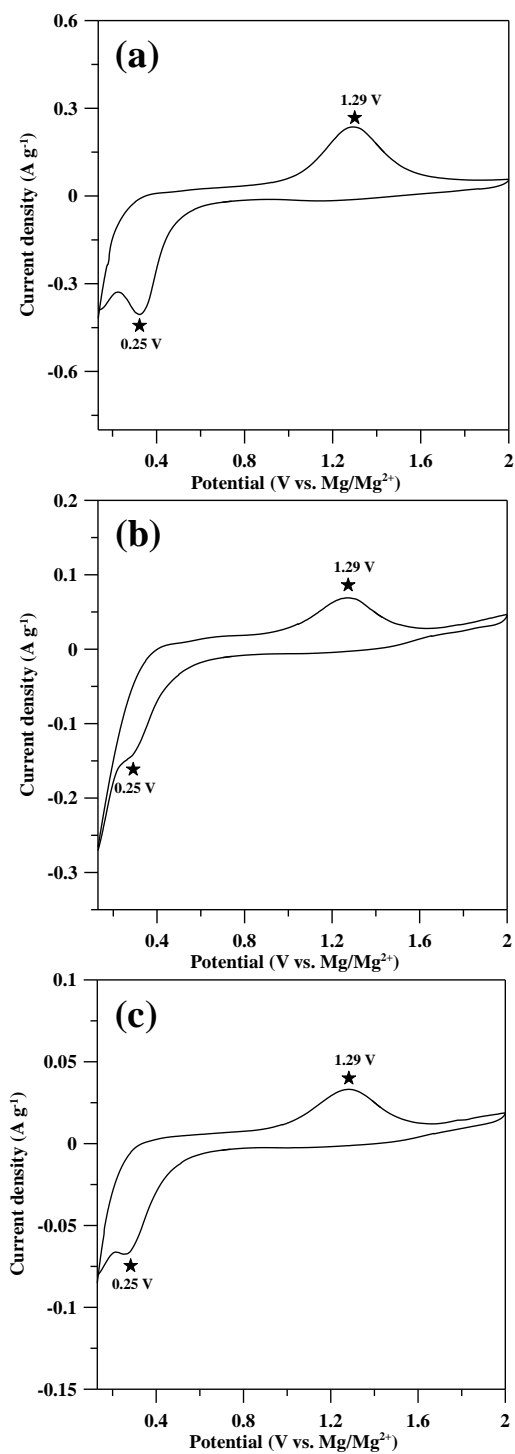Fig. 1. Typical XRD patterns of different composite cathodes.

Fig. 2.   FE-SEM micrographs of MgCo$_2$O$_4$/graphite composites with low and high

magnifications: (a,d) M3G7, (b,e) M5G5 and (c,f) M7G3 samples.

Fig. 3.   TEM images and elemental mapping pictures of (a) M3G7 (b) M5G5 and

(c) M7G3 samples, showing the presence and the distribution of C, Co, Mg,

and O elements on $MgCo_2O_4$/graphite composites.
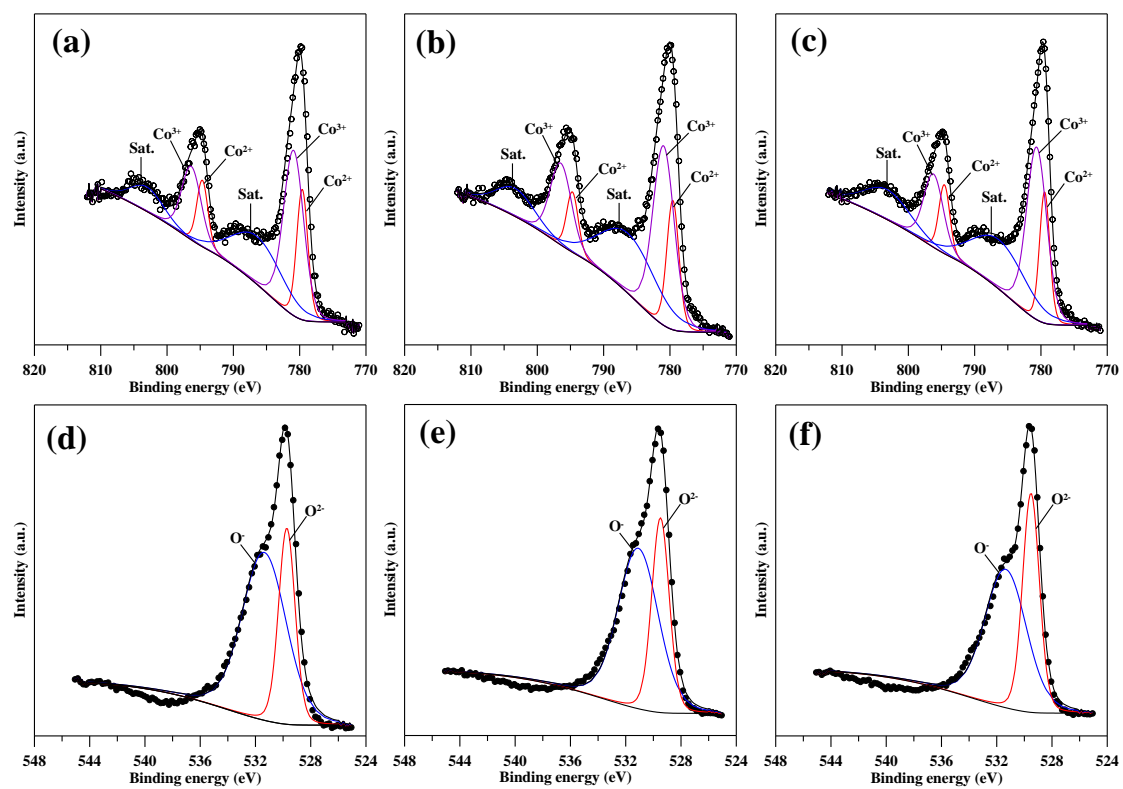
Figure 4.   XPS scan on Co 2p of MgCo$_2$O$_4$/graphite composites: (a) M3G7, (b) M5G5, and (c) M7G3. XPS scan on O 1s of MgCo$_2$O$_4$/graphite composites: (d) M3G7, (e) M5G5, and (f) M7G3.

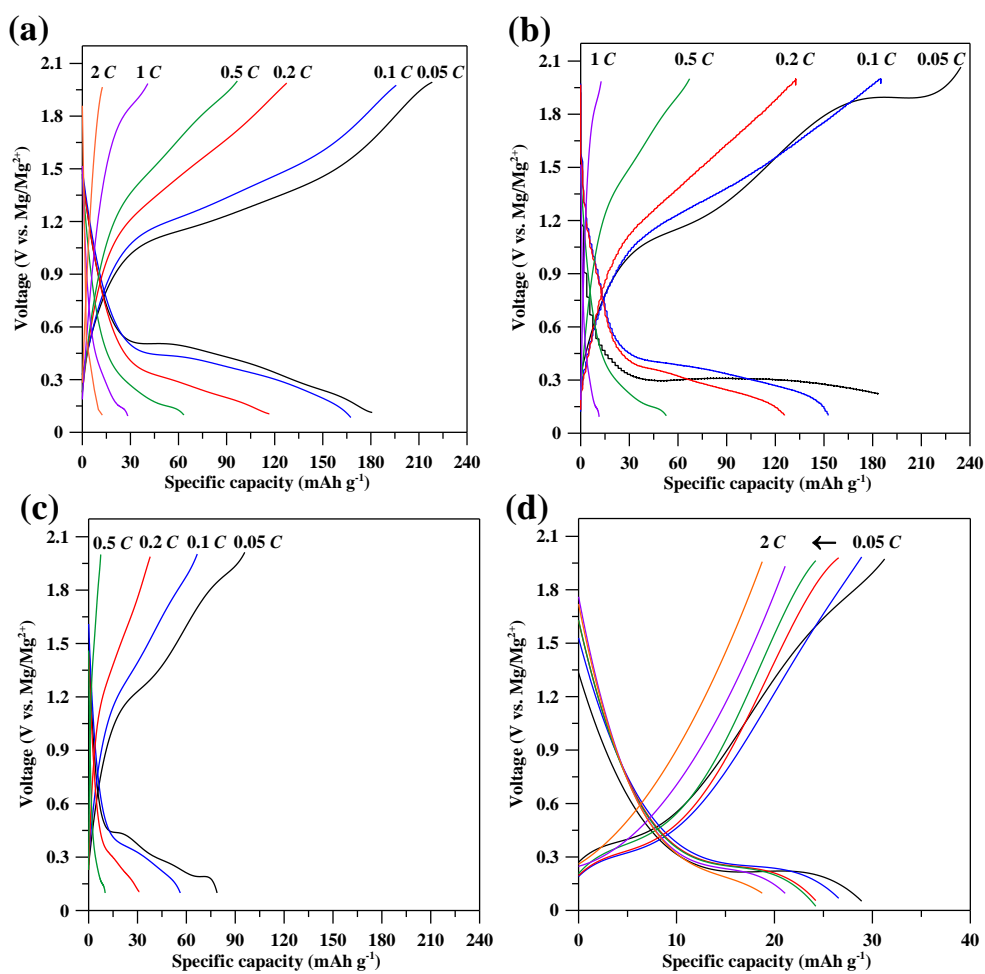Fig. 5. Typical CV curves of (a) M3G7, (b) M5G5 and (c) M7G3 electrodes.

Fig. 6.   Typical charge-discharge cycling curves of (a) M3G7, (b) M5G5, (c) M7G3

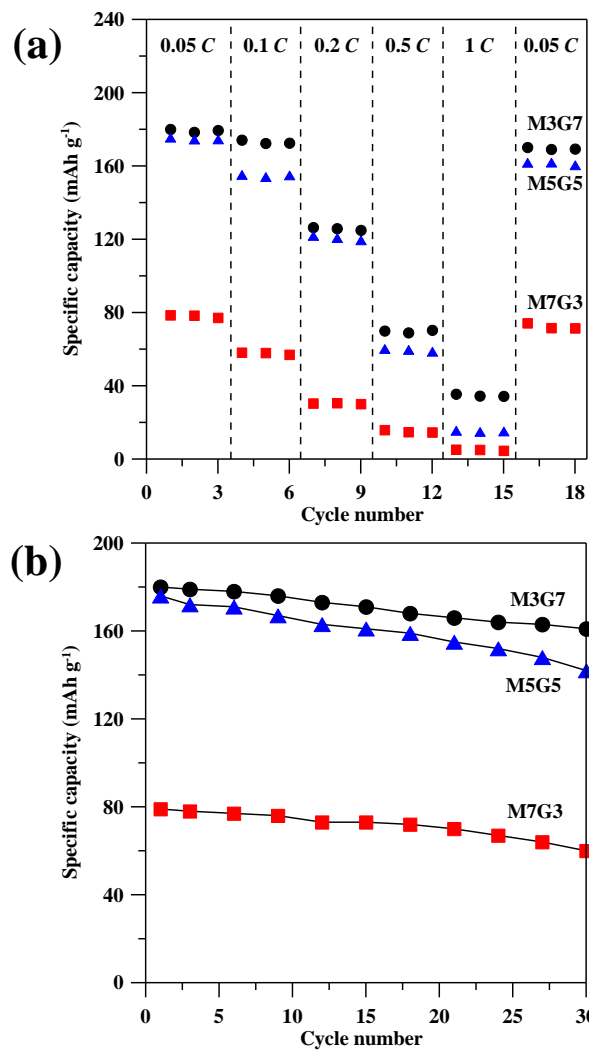and (d) graphite electrodes at different *C* rates.

Fig. 7.   (a) The discharge capacity of $MgCo_2O_4$/graphite electrodes as a function of cycle number at different C rates. (b) Cyclic stability of $MgCo_2O_4$/graphite electrodes charged and discharged at 0.05 C.
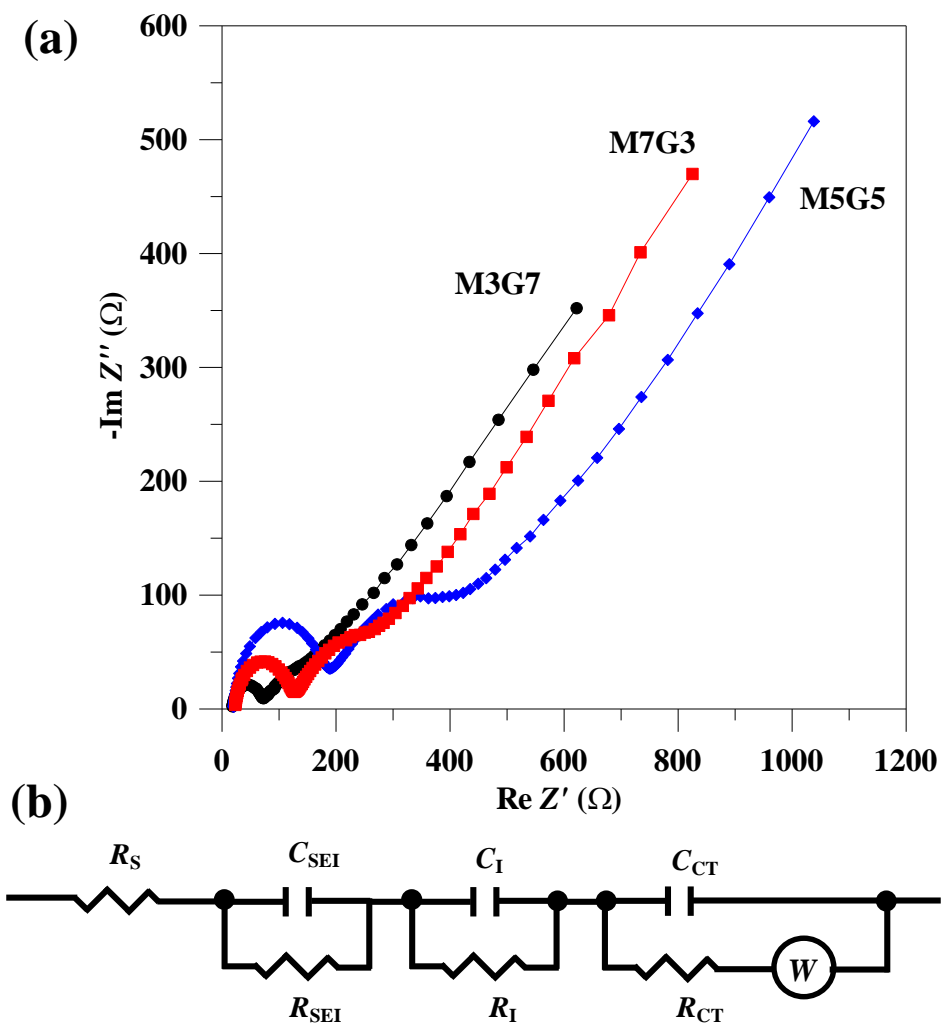
Fig. 8.   Electrochemical impedance spectroscopy of composite cathodes: (a)
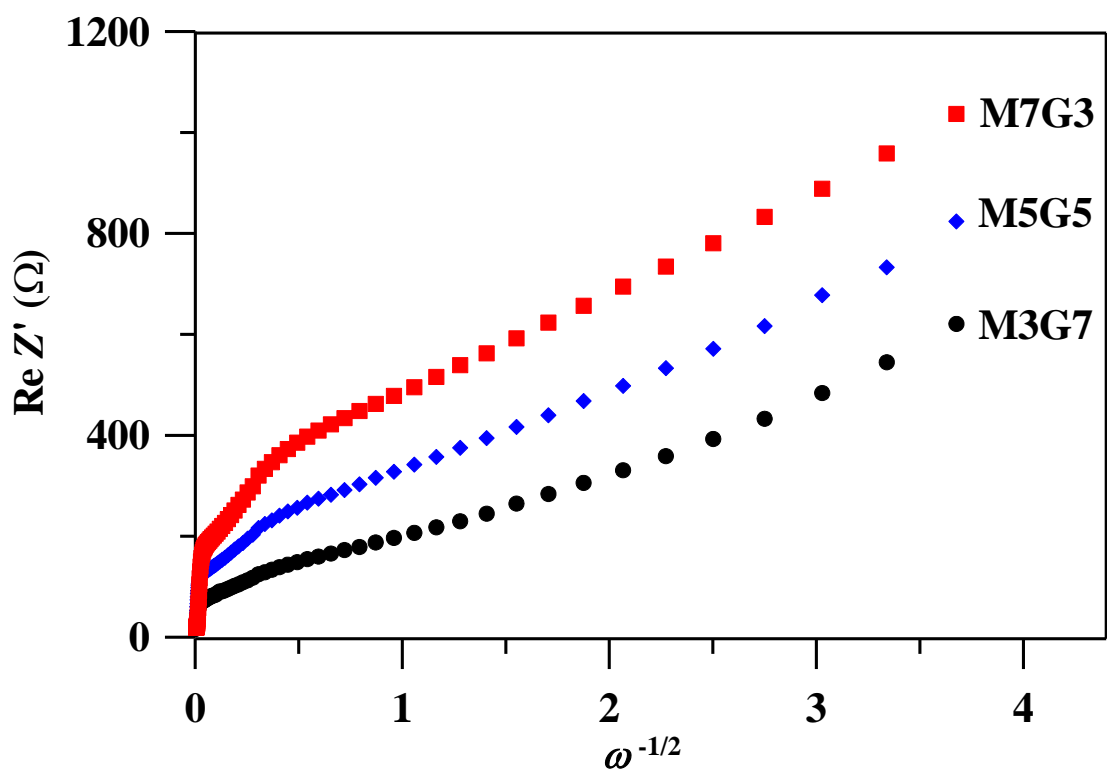
Nyquist plots and (b) equivalent circuit.

Fig. 9.   Randles plot of M3G7, M5G5 and M7G3 electrodes.